On the Lower Bound to the Input and Output Mismatch of Conditionally Stable Linear Two-Ports

IEEE Journal of Microwaves

Received 22 May 2023; accepted 19 June 2023. Date of publication 2 August 2023; date of current version 9 October 2023.

Digital Object Identifier 10.1109/JMW.2023.3289979

On the Lower Bound to the Input and Output Mismatch of Conditionally Stable Linear Two-Ports

GIOVANNI GHIONE (Life Fellow, IEEE), AND MARCO PIROLA (Senior Member, IEEE)

(Regular Paper)

Politecnico di Torino, Department of Electronics and Telecommunications, 10129 Torino, Italy

CORRESPONDING AUTHOR: Marco Pirola (e-mail: marco.pirola@polito.it).

This work was supported by the Regione Piemonte (Italy) through the European Radio Module for advancEd Spacecrafts (ERMES) Project.

ABSTRACT In the design of amplifier stages based on unconditionally stable linear active two-ports, the amplifier gain can be maximized through simultaneous conjugate matching with passive loads at the input and output ports. Conversely, the optimization of linear amplifiers based on conditionally stable active devices requires a trade-off between gain, stability margin, input/output port mismatch and (for low-noise amplifiers) noise figure. Exploiting potentially in-band unstable devices can be advantageous in the design of open-loop low-noise amplifiers, since the in-band stabilization with input resistors is well known to negatively affect the amplifier minimum noise figure. Within this framework, the article derives a lower bound to the input and output mismatch of non unconditionally stable linear two-ports. The minumum mismatch is shown to only depend, in a simple way, on the stability factor K and on the assumed mismatch ratio between the two ports. The minimum mismatch condition can be implemented by cascading the active, potentially in-band unstable two-port with two (input and output) reactive matching sections. The application of the theory to the design of low-noise amplifier open-loop stages based on conditionally stable active devices is discussed through CAD examples.

INDEX TERMS Circuit stability, input and output stability, linear circuits, scattering parameters, stability, stability criteria, two-port circuits.

I. INTRODUCTION

As well known, an unconditionally stable two-port with scattering matrix $\boldsymbol{S}'$ can be conjugately matched at both ports, at a certain frequency f, with passive loads, by cascading the two-port with an input (IM) and output (OM) reactive matching section, see Fig. 1, where $\boldsymbol{S}$ is the scattering matrix of the matched two-port. We assume that the two-port cascaded with the IM and OM sections is closed on the normalization resistance R_0 at both ports; thus, simultaneous conjugate matching implies $S_{11} = S_{22} = 0$ and $G = \text{MAG}$ where G is the two-port transducer (G_t), operational (G_p) or available (G_{av}) gain and MAG is the so-called maximum available gain.

Suppose now that the two-port with scattering matrix $\boldsymbol{S}'$ is potentially unstable (i.e., conditionally stable). In this case, gain maximization through simultaneous conjugate matching at the two ports with passive loads cannot be obtained [1], [2]: either port 1, or port 2, or both, will be mismatched. The problem we address here can be formulated as follows: is there a *lower bound* to the input and output mismatch that can be achieved, at a certain frequency f, by cascading the two-port with two reactive matching sections, as in Fig. 1, closed on the normalization resistance R_0? We will show, for the first time as far as our best knowledge goes, that the mismatch at the input an output port has a lower bound, whose value only depends on the Rollet stability parameter K [2] and the assumed mismatch ratio between the two ports, defined as:

$$\alpha = \begin{cases} |S_{22}| \,/\, |S_{11}| & \text{if} \quad |S_{22}| \le |S_{11}| \\ |S_{11}| \,/\, |S_{22}| & \text{if} \quad |S_{11}| \le |S_{22}| \end{cases}$$

where $\alpha \le 1$, provided that $-\alpha \le K \le 1$. Since the input and output matching sections are reactive, K is the same for the two two-ports characterized by the scattering matrices $\boldsymbol{S}$ and

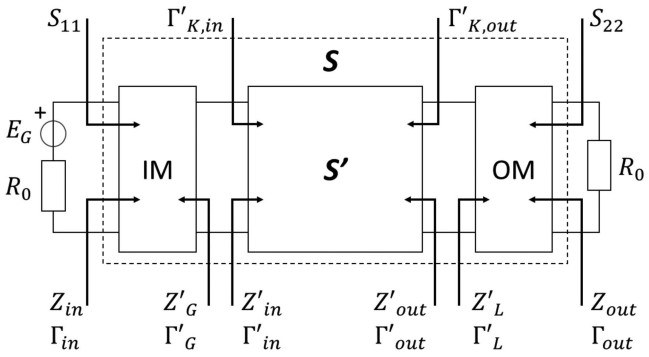

FIGURE 1. Two-port with scattering matrix S' cascaded with an input and output reactive matching section (IM and OM). The scattering matrix of the whole cascade is S. The two-port with matching sections is closed on the normalization resistance R_0 at the input and output ports.

$\boldsymbol{S}'$ [2]; therefore, the optimum matching condition derived from the stability factor K of $\boldsymbol{S}'$ also holds for $\boldsymbol{S}$ and can be implemented in the two-port having scattering matrix $\boldsymbol{S}$ through reactive input and output matching sections. We will also show that an infinity of solutions exist with minimum $|S_{11}|$ and $|S_{22}|$, but different S_{11} and S_{22} phases; moreover, all such solutions are characterized by the same G_t.

Design strategies for in-band conditionally stable narrowband (single-frequency) amplifiers based on a open-loop topology are discussed in the literature for the maximum gain [3, Sec. 3.7, "Potentially unstable bilateral case", p. 252 and 260] and the low-noise case [3, Examples 4.3.4 (p. 311) and 4.3.5 (p. 317)]. Such strategies are based on a tradeoff between input and output matching, gain, and, for low-noise amplifiers (LNAs), the noise figure (NF), obtained by selecting input and output terminations in the Smith chart stable region, also with the help of graphical aids, like the load (output) and generator (input) stability circles [3]. However, while the practically achievable maximum gain[1] or minimum NF, and corresponding optimum Γ'_G, are well known to the designer, no *a priori* knowledge is available so far of the minimum input and output mismatch which can be obtained from a given two-port by cascading it with reactive matching sections. This missing information obviously is a weak point in the design strategy, since the (so far unknown) optimum input and output matching achievable with a certain conditionally stable device could be incompatible altogether with the design optimization goals.

In practice, an interesting field for the application of potentially in-band unstable devices is represented by LNAs, since resistive input stabilization is detrimental to the amplifier NF;[2] a number of conditionally stable solutions are indeed available on the market [6]. Concerning the input and output mismatch, it is recognized in [3, Sec. 3.7, "Potentially unstable bilateral case", p. 252 and 260] that the input (output) matching can be improved by allowing for a larger output (input) mismatch. However, to our best knowledge, no *a-priori* estimate can be found in the literature on the minimum input and output mismatch that can be obtained in a conditionally stable two-port having certain stability parameters. The availability of such an estimate allows to devise a novel approach to LNA design exploiting conditionally stable devices, where, given the input/output mismatch ratio, the amplifier NF is optimized by selecting an input termination Z'_G leading to the minimum magnitude $|S_{11}|$ and $|S_{22}|$ but, at the same time, as close as possible to the optimum noise source termination (Z_{GNopt} or, equivalently, Γ_{GNopt}).

The article is structured as follows. After an introductory section (Section II) where we discuss the potential instability cases considered, we analyze first in Section III a specific case of minimum mismatch, i.e., a conditionally stable two-port, in which the output is matched and the input mismatch is minimized (or viceversa) through lossless matching sections. Section IV addresses instead the general case of a conditionally stable two-port, in which the minimum mismatch condition corresponding to a certain mismatch ratio α is derived. The computer-aided design (CAD) of the matching sections to achieve the minimum mismatch condition is discussed in Section V, while in Section VI we propose a low-noise amplifier CAD approach using, as case studies, a narrowband and 10% bandwidth low-noise FET amplifier stage. Conclusions are drawn in Section VII. Some analytical developments are reported in Appendix A (Section IX), Appendix B (Section X) and Appendix C (Section XI).

II. PRELIMINARY REMARKS

The present discussion is based on the two-parameter criterion [7], [8] as a necessary and sufficient condition for unconditional stability:

$$K = \frac{1 - |S_{22}|^2 - |S_{11}|^2 + |\Delta_S|^2}{2\,|S_{12}S_{21}|} > 1$$

$$|\Delta_S| = |S_{11}S_{22} - S_{12}S_{21}| < 1$$

The choice of the two-parameter stability criterion is motivated by the invariance of the stability factor K with respect to cascading with arbitrary reactive networks [2], that is not granted in single-parameter criteria [9] (i.e., the stability test is invariant, but the value of the stability parameter is not).

Another invariance property that will be exploited in the discussion is that of the Kurokawa reflection coefficients [10] at the ports of $\boldsymbol{S}'$ ($\Gamma'_{K,\text{in}}$ and $\Gamma'_{K,\text{out}}$, respectively):

$$\Gamma'_{K,\text{in}} = \frac{Z'_{\text{in}} - Z'^{*}_{G}}{Z'_{\text{in}} + Z'_{G}} \tag{1}$$

$$\Gamma'_{K,\text{out}} = \frac{Z'_{\text{out}} - Z'^{*}_{L}}{Z'_{\text{out}} + Z'_{L}} \tag{2}$$

[1] This should not be larger than the device maximum stable gain MSG = $|S'_{21}/S'_{12}|$, to keep Γ'_L and Γ'_G well within the stable region of the Smith chart [3].

[2] A popular LNA topology exploits a source series inductive feedback [4]; this has been shown to improve the device stability, at least in a certain inductance range [5], without overly affecting the NF. However, perfect simultaneous input and output matching of a conditionally stable device can only be obtained if the feedback inductor makes it unconditionally stable.

whose magnitude is invariant under lossless cascading, see, e.g., [3, Sec. 2.8, p. 199]. Thus, $|\Gamma'_{K,\text{in}}| = |S_{11}|$ and $|\Gamma'_{K,\text{out}}| = |S_{22}|$.

The restriction of K to the range $-\alpha \leq K \leq 1$, $0 \leq \alpha \leq 1$, is motivated as follows. While an unconditionally stable two-port can always be conjugately matched with passive loads, conjugate match is not a sufficient condition for unconditional stability in the case $K > 1$ but $|\Delta_S| > 1$; in fact, in such case matching with passive loads (that would correspond here to $S_{11} = S_{22} = 0$) is possible but corresponds to a minimum of the transducer gain G_t [3, Sec. 3.6 and Example 3.7.3]. For this reason, we will confine the treatment to the conditionally stable cases where $K < 1$. Moreover, as already mentioned, we will show that an optimum input and output matching condition only exists for $-\alpha \leq K \leq 1$, $0 \leq \alpha \leq 1$, implying that $K \geq -1$ anyway. Such limitation is consistent with the treatment in [11], [12], where it is demonstrated that if $K < -1$ either the input or the output are unconditionally unstable, see [12, Table II].

III. MATCHED PORT 2, MISMATCHED PORT 1 (OR VICEVERSA)

In the present section, we look for a lower bound of the input mismatch if the two-port is matched at the output port, i.e., $S_{22} = 0$, $S_{11} \neq 0$. This condition is commonly found in the design of LNA stages (irrespective of the device unconditional stability), where selecting a source impedance ($Z_{GN\text{opt}}$ or, equivalently, $\Gamma_{GN\text{opt}}$) corresponding to the minimum $\text{NF} = \text{NF}_{\text{min}}$ generally implies some input mismatch. The dual case (two-port matched at port 1 and mismatched at port 2) can be addressed by exchanging ports. We will consider the case $K < 1$ and $|\Delta_S| < 1$; as shown in Section IV, the latter condition indeed corresponds to minimum mismatch, see (17). Defining for brevity $A = S_{12}S_{21}$, the stability factor can be expressed as:

$$K = \frac{1 - |S_{11}|^2 + |S_{12}S_{21}|^2}{2\,|S_{12}S_{21}|} = \frac{1 - |S_{11}|^2 + |A|^2}{2\,|A|} \tag{3}$$

Given $K < 1$, the minimum $|S_{11}|$ as a function of $|A|$ can be readily found. In fact, starting from (3) and condition $K \leq 1$, we obtain:

$$|S_{11}|^2 = |A|^2 - 2\,|A|\,K + 1 \geq 0 \tag{4}$$

Equation (4) does not pose any limitations to the possible values of $|A|$ vs. K; in fact, $|A|^2 - 2|A|K + 1 \geq 0$ implies:

$$\frac{1}{2}\left(|A|^2 + 1\right) / |A| \geq K,$$

that is always true since:

$$\frac{1}{2}\left(|A|^2 + 1\right) / |A| \geq 1 \geq K \quad \forall\, |A|$$

Let us now find the minimum value of $|S_{11}|^2$ vs. $|A|$, corresponding to $|A| = |A|_{\text{opt}}$. By differentiating (4) we obtain:

$$\frac{\mathrm{d}\,|S_{11}|^2}{\mathrm{d}\,|A|} = 2\,|A| - 2K = 0 \rightarrow |A|_{\text{opt}} = K \tag{5}$$

The value $|A|_{\text{opt}}$ is certainly a minimum, since the second derivative of $|S_{11}|^2$ vs. $|A|$ is always positive. Moreover, since $|A|_{\text{opt}} > 0$, $|A|_{\text{opt}} = K$ is acceptable as a minimum if $0 \leq K \leq 1$; in such case, substituting into (4), we have:

$$|S_{11}|_{\text{min}} = \sqrt{1 - K^2} \tag{6}$$

We can therefore summarize the minimum conditions and related limitations for K as follows:

$$\begin{aligned} |S_{11}|_{\text{min}} &= \sqrt{1 - K^2}, \quad 0 \leq K \leq 1 \\ |A|_{\text{opt}} &\equiv |S_{12}S_{21}|_{\text{opt}} = K, \quad 0 \leq K \leq 1 \end{aligned}$$

which also implies $0 \leq |A|_{\text{opt}} \leq 1$. In the dual case where $S_{11} = 0$, $S_{22} \neq 0$ we have:

$$\begin{aligned} |S_{22}|_{\text{min}} &= \sqrt{1 - K^2}, \quad 0 \leq K \leq 1 \\ |A|_{\text{opt}} &\equiv |S_{12}S_{21}|_{\text{opt}} = K, \quad 0 \leq K \leq 1 \end{aligned}$$

A. DISCUSSION

The theory discussed above provides the optimum value of $|S_{12}S_{21}|$ and the minimum magnitude of $|S_{11}|$ ($S_{22} = 0$) or $|S_{22}|$ ($S_{11} = 0$) and, therefore, the minimum magnitude of the Kurokawa input (1) or output (2) reflection coefficients ($\Gamma'_{K,\text{in}}$ or $\Gamma'_{K,\text{out}}$), but not their phases. Thus, it may be expected that the solution in terms of Γ'_G or Γ'_L will not be unique. We will indeed show that the reflection coefficients Γ'_G and Γ'_L yielding constant magnitude of $\Gamma'_{K,\text{in}}$ and $\Gamma'_{K,\text{out}}$, respectively, lie on arcs of a circle corresponding to constant (available or operational) gain circles.

To illustrate this point, we exploit the case study from [3, Example 3.8.2 p.267], where a conditionally stable two-port with scattering matrix

$$\begin{aligned} S'_{11} &= 0.55\angle -120^\circ, \quad S'_{12} = 0.14\angle 30^\circ \\ S'_{21} &= 3.5\angle 60^\circ, \quad S'_{22} = 0.2\angle -50^\circ \end{aligned}$$

is matched at the input, while the output is mismatched so as to achieve an operational gain $G_p = 12$ dB. The stability factor is $K = 0.9474$ and $|\Delta_S| < 1$. In the original reference [3, Example 3.8.2 p.267], two possible solutions for the load are selected, $\Gamma'_{La} = 0.582\angle 50.05^\circ$ and $\Gamma'_{Lb} = 0.328\angle -143.98^\circ$. For these two cases, denoted as a and b, see Figs. 2 and 3, we have $|\Gamma'_{K,\text{out},a}| = 0.448$, $|\Gamma'_{K,\text{out},b}| = 0.447$, respectively.

For the sake of comparison, we scan the complex plane Γ'_L (for the definition of Γ'_L refer to Fig. 1), evaluating from the input reflection coefficient $\Gamma'_{\text{in}} = \Gamma'_{\text{in}}(\Gamma'_L)$ the matching generator reflection coefficient $\Gamma'_G = \Gamma'^*_{\text{in}}$. We then derive $\Gamma'_{\text{out}} = \Gamma'_{\text{out}}(\Gamma'_G)$, and from this $|\Gamma'_{K,\text{out}}|$. For each value of Γ'_L we also evaluate the operational gain $G_p(\Gamma'_L)$. The level curves of $|\Gamma'_{K,\text{out}}|$ and G_p (in dB) are presented in Figs. 2 and 3, respectively. It can be readily shown, see Appendix A (Section IX), that the constant gain and mismatch curves are circles, and that they coincide (i.e., Γ'_L values with the same $|\Gamma'_{K,\text{out}}|$ also have the same G_p).

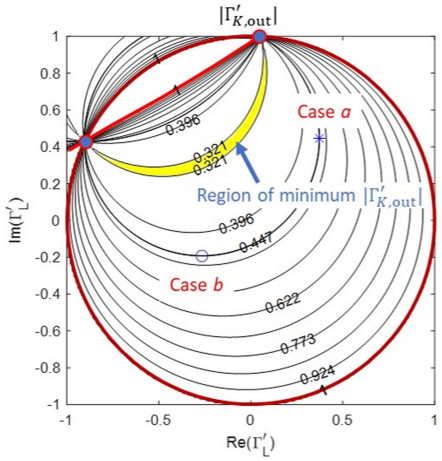

FIGURE 2. Level curves of $|\Gamma'_{K,\text{out}}|$ in the Γ'_L plane. Cases *a* and *b* are the solutions from [3, Example 3.8.2 p.267]; in the region with yellow shading indicated by the arrow $|\Gamma'_{K,\text{out}}| < 0.321$, close to the minimum value 0.3201. The range of Γ'_L values for which the level curves are shown is limited to unity. The thick red lines indicates the two circles where $\Gamma'_L = 1$, which occurs on the unit circle of the Γ'_L plane and in a arc of circle located in the left hand top of the Smith Chart. The two curves cross at the so-called *invariant points* (blue dots, see Appendix A).

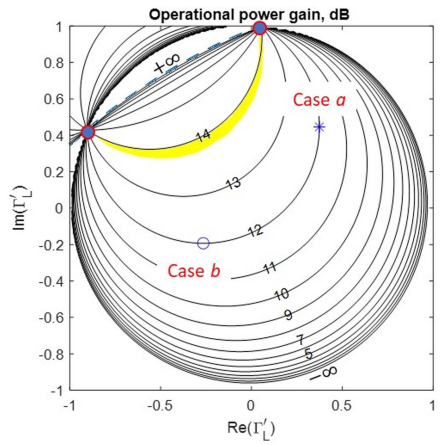

FIGURE 3. Level curves of G_p in the Γ'_L plane. Cases *a* and *b* are the solutions from [3, Example 3.8.2 p.267]. The blank regions outside or inside the Smith chart correspond to unstable regions where $G_p < 0$; in particular the arc of circle (blue dashed line) in the topmost left part of the Smith chart where $G_p \to \infty$ coincides with the output (or load) stability circle. The region with yellow highlight corresponds to the minimum locus of $|\Gamma'_{K,\text{out}}|$.

In Fig. 2, we can identify a crescent-shaped region (highlighted in yellow) where $|\Gamma'_{K,\text{out}}|$ is close (i.e., with a difference $< 10^{-3}$ in magnitude) to the minimum, equal to $\sqrt{1-K^2} = \sqrt{1-0.9474^2} = 0.3201$. All points of the Γ'_L plane belonging to the minimum arc of circle lying within the unit circle (and therefore corresponding to stable loads) can be transformed into R_0, leading to an *infinity of solutions*. Cases *a* and *b* in Figs. 2 and 3 correspond to a larger output reflection coefficient than the minimum one. Selecting the load according to the optimum theoretical matching with $|\Gamma'_{K,\text{out}}| = 0.3201$ would have led to an operational gain of about 14 dB (corresponding to the device MSG) instead of 12 dB (the value suggested in [3, Example 3.8.2 p.267]), as it can be seen from Fig. 3. While, in this case, all loads leading to minimum $|\Gamma'_{K,\text{out}}|$ are equivalent (since they correspond to the same G_p), further constraints (like the minimization of the NF) can drive the design towards selecting a specific point of the minimum reflection coefficient arc of circle, see Section VI.

In conclusion, when transforming R_0 into the value of Z'_G ($|S_{22}| = 0$ case) or Z'_L ($|S_{11}| = 0$ case) yielding $|\Gamma'_{K,\text{in}}| = |S_{11}|_{\min}$ or $|\Gamma'_{K,\text{out}}| = |S_{22}|_{\min}$, respectively, an infinity of solutions can be obtained. In case of output mismatch and input matching, those solutions are characterized by the same operational power gain, as seen in the previously discussed example; in case of input mismatch and output matching, by the same available power gain G_{av}.[3]

IV. ASSIGNED MISMATCH RATIO AT PORTS 1 AND 2

In this section, we show that optimum matching at the input and output ports (and also the range of values of K where this matching can be achieved) generally depends on the mismatch ratio α and on the value of the stability parameter K. In other words, the magnitude of the reflection coefficients at the two ports ($|S_{11}|$ and $|S_{22}|$) cannot be minimized independently. We therefore assume $|S_{11}| = \Gamma$, $|S_{22}| = \alpha\Gamma$, where $\alpha \geq 0$ is the assigned mismatch ratio, and look for a lower bound of Γ. Without loss of generality, we assume $\alpha \leq 1$; since K is invariant under exhange of the two ports, the solution found will hold also in the case where $|S_{11}| \leq |S_{22}|$, see (18) and (19).

For brevity, we define again $S_{12}S_{21} = A$ and denote as ψ the phase of $S_{11}S_{22}$ (i.e., $S_{11}S_{22} = \alpha\Gamma^2 \exp(\mathrm{j}\psi)$). The case examined in Section III corresponds to $\alpha = 0$; if $\alpha = 1$ the same mismatch is assumed at the two ports. The stability factor K can be now expressed as:

$$K = \frac{1 - |S_{22}|^2 - |S_{11}|^2 + |S_{11}S_{22} - S_{12}S_{21}|^2}{2\,|S_{12}S_{21}|} = \\ = \frac{1 - \left(1+\alpha^2\right)\Gamma^2 + \left|\alpha\Gamma^2 \exp(\mathrm{j}\psi) - A\right|^2}{2\,|A|} = \\ = \frac{1 - \left(1+\alpha^2\right)\Gamma^2 + \alpha^2\Gamma^4 + |A|^2 - 2\alpha\Gamma^2\,|A|\cos\phi}{2\,|A|} \quad (7)$$

where ϕ is the angle between $\alpha\Gamma^2 \exp(\mathrm{j}\psi)$ and A. It is straightforward to show that, given K and $|A|$, the minimum Γ corresponds to $\phi = 0$, i.e., $\cos\phi = 1$. In fact, from (7) we obtain:

$$\left|\alpha\Gamma^2 \exp(\mathrm{j}\psi) - A\right|^2 = 2\,|A|\,K - 1 + \left(1+\alpha^2\right)\Gamma^2 \geq 0,$$

where the term $|\alpha\Gamma^2 \exp(\mathrm{j}\psi) - A|^2$ is minimum when $\alpha\Gamma^2 \exp(\mathrm{j}\psi)$ is in phase with A or $\cos\phi = 1$. If this term

[3]Note that, having assigned specific values of Z'_G or Z'_L, yet another infinity of equivalent $\boldsymbol{S}$ solutions can be generated by reference plane shift at the input and output ports.

is minimum, also $2|A|K - 1 + (1+\alpha^2)\Gamma^2$ is minimum, but with fixed $|A|$, α and K also Γ^2 and therefore Γ is minimum. Thus $\Gamma \equiv \Gamma_a$ is minimized, given K, α and $|A|$, when $\phi = 0$. In such conditions:

$$K = \frac{1 - \left(1+\alpha^2\right)\Gamma_a^2 + \left(\alpha\Gamma_a^2 - |A|\right)^2}{2\,|A|} \tag{8}$$

We can generally derive Γ_a given K, $|A|$ and α with $\cos\phi = 1$ by solving a quadratic equation in Γ_a^2, since from (8) we obtain:

$$\alpha^2\Gamma_a^4 - \Gamma_a^2\left(1 + \alpha^2 + 2\alpha\,|A|\right) + 1 + |A|^2 - 2\,|A|\,K = 0 \tag{9}$$

As shown in Appendix B, the only solution of (9) admitting values within the Smith chart is:

$$\Gamma_- = \sqrt{a - b}, \tag{10}$$

$$a = \frac{2\,|A|\,\alpha + \alpha^2 + 1}{2\alpha^2} \tag{11}$$

$$b = \frac{\sqrt{\left(1-\alpha^2\right)^2 + 4\,|A|\left(\alpha + 2K\alpha^2 + \alpha^3\right)}}{2\alpha^2} \tag{12}$$

For $\alpha = 0$ we again obtain the expression in (6). Since, as discussed in Appendix B, Γ_-^2 is positive, the minimum reflection coefficient can be obtained by minimizing Γ_-^2. Differentiating, we have, for $\alpha \neq 0$:

$$\frac{\mathrm{d}\Gamma_-^2}{\mathrm{d}\,|A|} = \frac{1}{\alpha} - \frac{1 + 2K\alpha + \alpha^2}{\alpha\sqrt{\left(1-\alpha^2\right)^2 + 4\,|A|\left(\alpha + 2K\alpha^2 + \alpha^3\right)}} = 0$$

that leads, for $-\alpha \le K \le 1$, to the solution:

$$|A|_{\mathrm{opt}} \equiv |S_{12}S_{21}|_{\mathrm{opt}} = \frac{K\alpha^2 + \left(1+K^2\right)\alpha + K}{\alpha^2 + 2K\alpha + 1}, \tag{13}$$

$$\Gamma_{\min} = \sqrt{\frac{1-K^2}{\alpha^2 + 2K\alpha + 1}}, \tag{14}$$

where (13) tends to (5) when $\alpha \to 0$. The extreme found is a minimum, as it is readily demonstrated by discussing the sign of the second derivative of Γ_-^2 vs. $|A|$, that is always positive. Notice that $\Gamma_{\min} = 0$ for $K = 1$ and $\Gamma_{\min} = 1$ for $K = -\alpha$; therefore, the range of K allowing for partial matching at the two ports is $-\alpha \le K \le 1$, and, correspondingly, $0 \le |A|_{\mathrm{opt}} \le 1$. Outside the range $-\alpha \le K \le 1$ the solution found is unphysical, or anyway unstable, see Appendix C, in agreement with [11], [12].

We show now that $\Gamma_{\min} \le 1$ always. Since $\alpha^2 + 2K\alpha + 1 \ge 0$ for $-\alpha \le K$, we have that the argument of the square root in (14) is below unity, since it always satisfies the following implication chain:

$$\frac{1-K^2}{\alpha^2 + 2K\alpha + 1} \le 1 \rightarrow 1 - K^2 \le \alpha^2 + 2K\alpha + 1 \rightarrow$$

$$\rightarrow \alpha^2 + 2K\alpha + K^2 = (\alpha + K)^2 \ge 0$$

Thus, $\Gamma_{\min} \le 1$, corresponding to passive terminations:

$$|S_{11}|_{\min} = \Gamma_{\min} \tag{15}$$

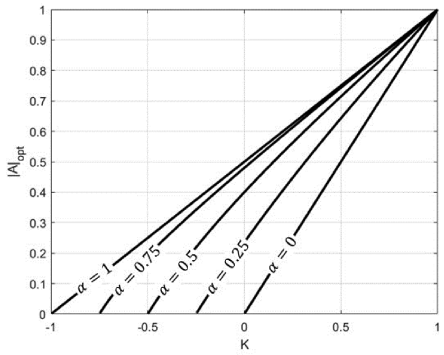

FIGURE 4. Behavior of $|A|_{\mathrm{opt}}$ vs. K for different values of the relative mismatch parameter α.

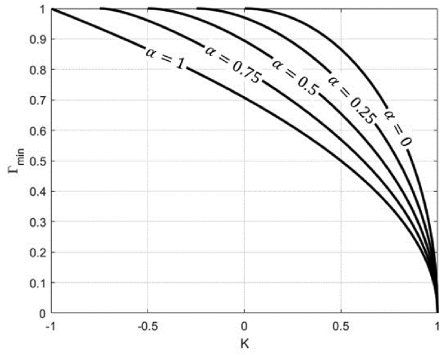

FIGURE 5. Behavior of $\Gamma_{\min}$ vs. K for different values of the relative mismatch parameter α.

$$|S_{22}|_{\min} = \alpha\Gamma_{\min} \tag{16}$$

within the Smith chart. We may also derive the $|\Delta_S|_{\mathrm{opt}}$ corresponding to the minimum mismatch, and confirm that $|\Delta_S|_{\mathrm{opt}} \le 1$. Taking into account that $S_{11}S_{22} = \alpha\Gamma^2\exp(\mathrm{j}\psi)$ and A are in phase, we have, for $-\alpha \le K \le 1$,

$$\begin{aligned} |\Delta_S|_{\mathrm{opt}} &= \left|\alpha\Gamma_{\min}^2\exp(\mathrm{j}\psi) - A_{\mathrm{opt}}\right| \\ &= \left|\alpha\Gamma_{\min}^2 - |A|_{\mathrm{opt}}\right| = |K| \le 1 \end{aligned} \tag{17}$$

In the case considered, we have looked for a minimum mismatch under the assumption $|S_{22}| \le |S_{11}|$; since the solution is invariant (due to the invariance of K and $|A|_{\mathrm{opt}}$) by exchanging ports 1 and 2 we also have:

$$|S_{11}|_{\min} = \alpha\Gamma_{\min} \tag{18}$$

$$|S_{22}|_{\min} = \Gamma_{\min} \tag{19}$$

that covers the case where we look for a minimum mismatch assuming $|S_{22}| \ge |S_{11}|$.

The theoretical values of $|A|_{\mathrm{opt}}$, $\Gamma_{\min}$ and $\alpha\Gamma_{\min}$ are presented in Figs. 4–6, respectively, as a function of K ($-\alpha \le K \le 1$) and for different values of the parameter α. In general, $\Gamma_{\min}$ increases with decreasing K, and the best compromise between input and output matching, and also the broadest range of possible values of K, occurs (not unexpectedly) for

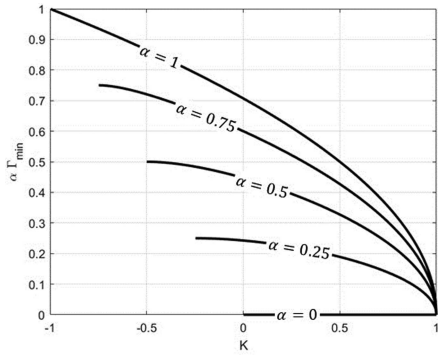

FIGURE 6. Behavior of $\alpha\Gamma_{\min}$ vs. K for different values of the relative mismatch parameter α.

$\alpha = 1$ where:

$$|S_{11}|_{\min} = |S_{22}|_{\min} = \Gamma_{\min} = \sqrt{\frac{1-K}{2}}, \quad -1 \le K \le 1$$

$$|A|_{\text{opt}} \equiv |S_{12}S_{21}|_{\text{opt}} = \frac{K+1}{2}, \quad -1 \le K \le 1$$

We finally note that the transducer gain of $\boldsymbol{S}$ (that is closed on its normalization resistances) $G_t \equiv |S_{21}|^2$ is independent of the choice of input and output matching sections (and therefore of Z'_G and Z'_L) leading to minimum mismatch. In fact, $|S_{12}S_{21}| = |S_{12}S_{21}|_{\text{opt}}$ only depends on K and α, see (13), not on the specific minimum mismatch solution; moreover, $S_{21}/S_{12} = S'_{21}/S'_{12}$ always, since this parameter is invariant under reciprocal network cascading [13, Ch. 8 and 9]. It follows that the transducer gain of $\boldsymbol{S}$:

$$G_t \equiv |S_{21}|^2 = \left|\frac{S_{21}}{S_{12}}\right| |S_{12}S_{21}| \equiv \left|\frac{S'_{21}}{S'_{12}}\right| |S_{12}S_{21}|_{\text{opt}}$$

is invariant with respect of the choice of one of the infinite optimum Z'_G and Z'_L solutions that may be obtained through optimization.

V. CAD IMPLEMENTATION

While Smith chart maps of the magnitude of the output or input reflection coefficient like that in Fig. 2 are useful to understand the location and properties of the minimum mismatch locus,[4] the design of the matching networks is conveniently performed through CAD-assisted optimization. However, the minimization of the input and output mismatch has to be carried out with care, because the solution is not unique even when the theoretical minimum is imposed as an optimiziation goal; this may lead to matching sections with uselessly inconvenient parameters. Even worse, if this minimum is not previously known, the (unweighted) two-goal optimization process could lead to an unpredictable value of the mismatch ratio, that would in turn decide on the minimum achievable matching.

[4]The minimum mismatch generator and load reflection coefficients are always located in the stable region of the Smith chart, since they correspond, in the matched two-port, to S_{11} and S_{22} being below unity in magnitude.

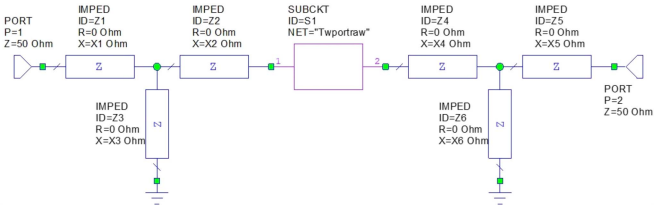

FIGURE 7. Adopted structure of the input and output matching sections.

In practice, to implement in a CAD environment the minimum matching search, we exploit the following strategy for $\alpha = 0$ (Section III) and arbitrary α (Section IV).

In case $\alpha = 0$ (for the sake of definiteness, we assume a matched output, mismatched input port), we evaluate the stability factor K and from it the minimum $|S_{11}|$ and optimum $|A|$. Then, we add two reactive matching sections at the input and output, and numerically optimize them by imposing as a constraint an output mismatch as low as possible and an input mismatch corresponding to the theoretical $|S_{11}|_{\min}$; since $|A|_{\text{opt}}$, $|S_{11}|_{\min}$ and K are related by (4), and the stability factor K is invariant when cascading the two-port with scattering matrix $\boldsymbol{S}'$ with reactive matching sections, this would also yield $|A|_{\text{opt}}$. As already noticed, the solution we obtain in terms of matching sections is not unique, since the phase of $S_{11\,\min}$ and of $A_{\text{opt}} = (S_{12}S_{21})_{\text{opt}}$ is arbitrary. This means that, without further constraints (e.g., on the NF), the solution obtained will depend on the starting values of the optimization parameters. However, all solutions will have the same available power gain.

For arbitrary α, the optimization procedure consists in imposing $|S_{11}| = \Gamma_{\min}$, $|S_{22}| = \alpha\Gamma_{\min}$. Also in this case, the phases of the minimum S_{11}, S_{22} and $A_{\text{opt}} = (S_{12}S_{21})_{\text{opt}}$ are not uniquely defined, leading to an infinity of possible solutions corresponding to different matching sections, but, again, if the minimum condition is met, all solutions will have the same G_t. An alternative optimization strategy (that is feasible if the CAD tool used supports the definition of optimization parameters through user-defined formulae) consists in assigning the mismatch ratio α and directly minimize the parameter Γ.

The procedure was tested first with a set of randomly generated conditionally stable scattering matrices with $-1 \le K \le 1$; the input and output matching sections are chosen as constant reactance T-sections, see Fig. 7; as well known, this choice is redundant (i.e., a proper L-section is enough for single-frequency matching), but has been adopted to automatize the optimization process. The results, not reported here for brevity, confirm that, using the simplex optimizer of a commercial RF design suite, the optimized reflection coefficients indeed exactly correspond in magnitude to the theoretical values, and that the solution is not unique.

VI. LNA DESIGN

We discuss here a design strategy for open-loop LNAs based on in-band conditionally stable devices. First we report two

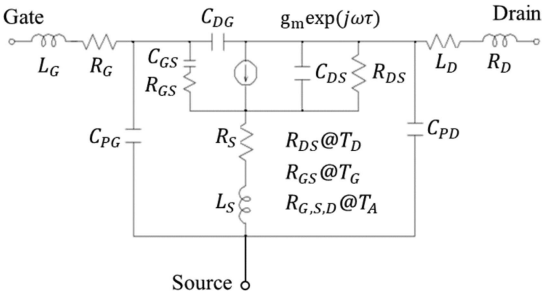

FIGURE 8. Small-signal equivalent circuit of the FET considered in Sections VI-A and VI-B; the noise model is a two-temperature model [14]. The model parameters are: $g_m = 100$ ms, $\tau = 0$ ns; $R_{GS} = 4\ \Omega$, $R_{DS} = 300\ \Omega$, $R_S = 3\ \Omega$, $R_D = 3\ \Omega$, $R_G = 3\ \Omega$; $C_{GS} = 0.25$ pF, $C_{DS} = 0.05$ pF, $C_{DG} = 0.05$ pF, $C_{PG} = 0.01$ pF, $C_{PD} = 0.01$ pF; $L_S = 0.01$ nH, $L_D = 0.1$ nH, $L_G = 0.2$ nH; $T_A = 23.85$ °C, $T_G = 23.85$ °C, $T_D = 1727$ °C.

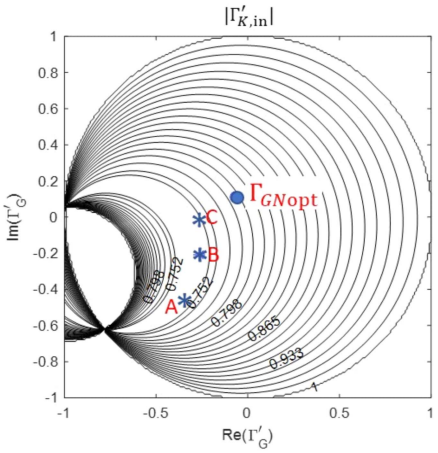

FIGURE 9. Level curves of the input Kurokawa reflection coefficient magnitude $|\Gamma'_{K,\mathrm{in}}|$ in the source reflection coefficient plane Γ'_G; the star markers denote cases A B and C. All points lay in a region where $|\Gamma'_{\mathrm{in}}| < 0.752$, the minimum being 0.74, see Table 1. $\Gamma_{G\mathrm{opt}}$ is the optimum noise source reflection coefficient. Notice that the range of Γ'_G values for which the level curves are shown is limited to unity.

practical examples: a FET-based LNA stage at 20 GHz (Section VI-A) covering cases $\alpha = 0$ and $\alpha = 1$, and a 10% bandwidth stage, based on the same device (Section VI-B), with $\alpha = 1$. Then, the proposed design strategy is generalized and summarized in Section VI-C.

A. LOW-NOISE FET NARROWBAND STAGE

We consider here a microwave FET characterized with a standard small-signal equivalent circuit and two-temperature noise model [14], whose scheme is shown in Fig. 8; the intrinsic cutoff frequency is around 64 GHz, compatible with a 20 GHz LNA stage design. At $f = 20$ GHz the simulated scattering parameters are

$$S'_{11} = -0.6359 + 0.2106\mathrm{j}, \quad S'_{12} = 0.1622 - 0.0425\mathrm{j}$$
$$S'_{21} = 1.3034 + 1.5547\mathrm{j}, \quad S'_{22} = -0.2171 - 0.2528\mathrm{j}$$

The minimum noise figure is $\mathrm{NF}_{\min} = 1.37$, the associated gain $G_{\mathrm{ass}} \equiv G_{av}(\Gamma_{NG\mathrm{opt}}) = 4.73$, $\Gamma_{NG\mathrm{opt}}$ optimum noise source reflection coefficient, the stability factor $K = 0.67$.

We discuss first the case $\alpha = 0$, where the output port is matched and the input port matching section is optimized so as to obtain the minimum input reflection coefficient. To show that the already mentioned non-uniqueness of the solution can be exploited to optimize both the input reflection coefficient and the NF, we systematically explore the whole Γ'_G plane, imposing, for each point, the output matching: the output reflection coefficient was optimized to be approximately equal to -50 dB. The cases considered for $\alpha = 0$ are denoted as case A, B and C, see Fig. 9; all of them exhibit a mismatch close to the minimum one (i.e., within $\approx 1\%$), but are increasingly close to the optimum noise source reflection coefficient $\Gamma_{GN\mathrm{opt}}$.[5] Points A and B were obtained without using as a further optimization goal the minimization of NF, while for point C the NF minimization was considered together with the theoretical optimum matching. The results are shown in Table 1, where we see that for points A and B the optimized

TABLE 1. Parameters of the Input and Output Matching Sections (above) and Performance for Cases A, B, C and D (below)

Case	X_1, Ω	X_2, Ω	X_3, Ω	X_4, Ω	X_5, Ω	X_6, Ω
A	121.37	-96.16	167.87	-6.02	44.37	110.24
B	60.27	-63.46	180.28	-5.29	20.14	70.23
C	82.66	67.97	280.32	-14.58	29.10	81.56
D	98.23	-65.74	134.62	-13.18	4.92	73.86

Case	NF	G_a	G_t	$\lvert\Gamma'^{,\mathrm{sim.}}_{K,\mathrm{in}}\rvert$	$\lvert\Gamma'^{,\mathrm{sim.}}_{K,\mathrm{out}}\rvert$	$\lvert\Gamma'^{,\mathrm{th.}}_{K,\mathrm{in}}\rvert$	$\lvert\Gamma'^{,\mathrm{th.}}_{K,\mathrm{out}}\rvert$
A	1.80	7.49	7.49	0.74	0.0031	0.74	0
B	1.48	7.44	7.44	0.74	0.0032	0.74	0
C	1.41	6.63	6.63	0.75	0.0032	0.74	0
D	1.61	11.09	9.23	0.41	0.41	0.41	0.41

reflection coefficient coincides with the theoretical optimum, while in point C the lowest NF compatible with the optimum matching is obtained, with a slight matching penalty and a larger penalty in the gain, as seen from Fig. 10. Notice that, while the input reflection coefficient increases only weakly in the region close the minimum, the gain quickly decreases when moving away from the optimum matching region towards $\Gamma_{GN\mathrm{opt}}$.

If the optimum input matching obtained in Cases A-C is too poor, the only way to improve it without increasing the device K consists in allowing for some output mismatch. Indeed, the best input matching can be obtained by imposing the same mismatch at the input and output ports, i.e., for $\alpha = 1$, corresponding to Case D.

To graphically discuss this case, we scan the entire Γ'_G plane, and impose, for each value, $|\Gamma'_{K,\mathrm{in}}| = |\Gamma'_{K,\mathrm{out}}| = \Gamma_{\min}$ by properly selecting Γ'_L. The matching sections shown in Table 1 for Case D are obtained by imposing, with equal optimization weights, both $|\Gamma'_{K,\mathrm{out}}| = |\Gamma'_{K,\mathrm{in}}| = \Gamma_{\min}$ and NF as close as possible to the minimum. As a result, as shown in Fig. 11, out of the infinite optimum solutions in the Γ'_G plane, we select the one closest to $\Gamma_{GN\mathrm{opt}}$. Compared to cases A-C, in

[5] As well known, the NF deviation vs. the optimum (minimum) value is proportional to $|\Gamma'_G - \Gamma'_{GN\mathrm{opt}}|^2$, see e.g. [3, Sec. 4.3].

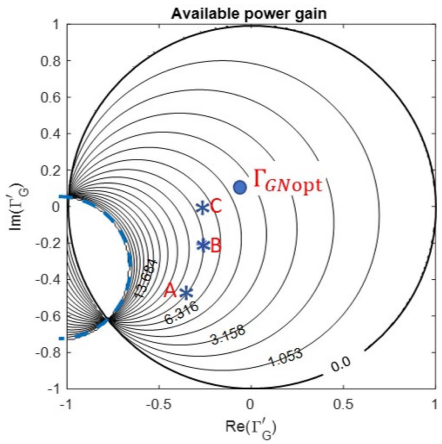

FIGURE 10. Level curves of the available power gain G_{av} as in the source reflection coefficient plane Γ'_G; the star markers denote cases A B and C. Γ_{GNopt} is the optimum noise source reflection coefficient. The blue dashed arc of circle where $G_{av} \to \infty$ is the input stability circle.

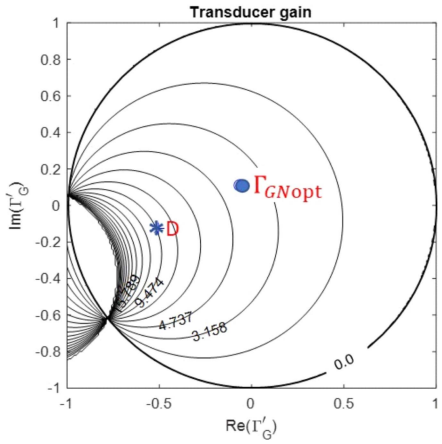

FIGURE 12. Level curves of the transducer gain G_t in the source reflection coefficient plane Γ'_G; the asterisk denotes case D. Γ_{GNopt} is the optimum noise generator reflection coefficient.

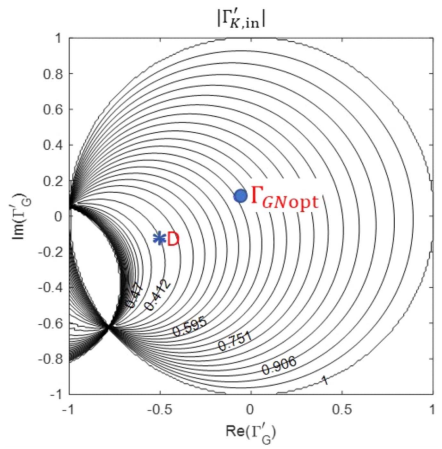

FIGURE 11. Level curves of the input Kurokawa reflection coefficient magnitude $|\Gamma'_{K,\mathrm{in}}|$ in the source reflection coefficient plane Γ'_G; the asterisk denotes case D. Γ_{GNopt} is the optimum noise source reflection coefficient. Notice that the range of Γ'_G values for which the level curves are shown is limited to unity.

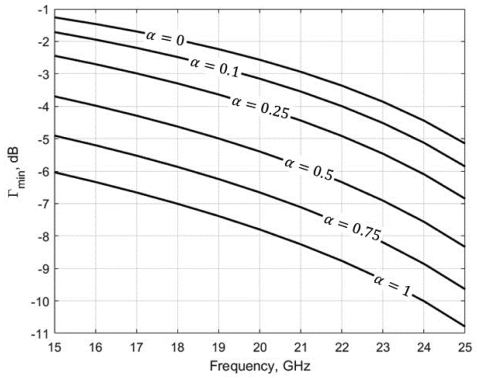

FIGURE 13. Minimum theoretical reflection coefficient at the input port Γ_{min} as a function of the frequency for the equivalent circuit in Fig. 8 for different values of the mismatch ratio α.

case D the input matching and the transducer gain are better, at the expense of a worse output reflection coefficient and NF, see Fig. 12 and Table 1, where G_t is evaluated using the load termination resulting from the minimum search already described.

B. LOW-NOISE FET STAGE WITH 10% BANDWIDTH

The theoretical lower bounds derived as a function of the mismatch ratio and stability factor K can be also conveniently exploited in the in-band optimization of a wider band LNA. As a case study, we consider the design of a 10% bandwidth LNA stage based on the FET with equivalent circuit in Fig. 8. We set the LNA optimization targets as follows: 10% bandwidth around 20 GHz (i.e., 19-21 GHz) with transducer gain flatness ±0.5 dB, NF lower than 1.5, input and output reflection coefficients of −6 dB at least.

As a first step, we have to check whether the matching requirements are compatible with the theoretical minimum mismatch on the whole amplifier bandiwdth, taking into account that the stability factor is frequency dependent. From the equivalent circuit and the related S-parameters we obtain that the K factor increases almost linearly from $K = 0.5$ (15 GHz) to $K = 0.83$ (25 GHz). The $|S_{11}| = \Gamma_{\mathrm{min}}$ and $|S_{22}| = \alpha\Gamma_{\mathrm{min}}$ minimum reflection coefficients given by (14) vary in frequency as shown in Figs. 13 and 14. Since K increases with frequency, as expected, thus improving the device stability, Γ_{min} and $\alpha\Gamma_{\mathrm{min}}$ decrease with frequency. We have therefore to consider as a worst case the mismatch value in the lower frequency limit (19 GHz). Matching port 2 ($\alpha = 0$) would correspond to an input reflection coefficient of only about −2.2 dB at 19 GHz, that is unacceptably low. To leave some margin to the optimization of other parameters, we select the best possible condition of mismatch ratio, i.e., $\alpha = 1$, where

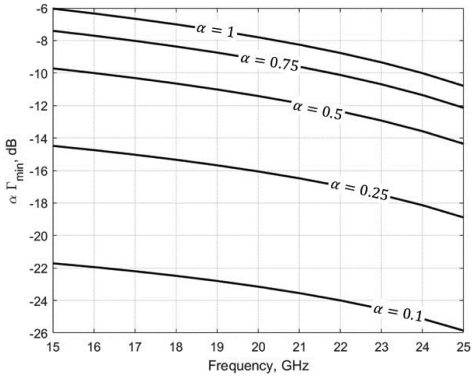

FIGURE 14. Minimum theoretical reflection coefficient at the output port $\alpha\Gamma_{min}$ as a function of frequency for the equivalent circuit in Fig. 8 for different values of the mismatch ratio α. The value for $\alpha = 0$ is not shown, since it would correspond to $-\infty$ in a log scale.

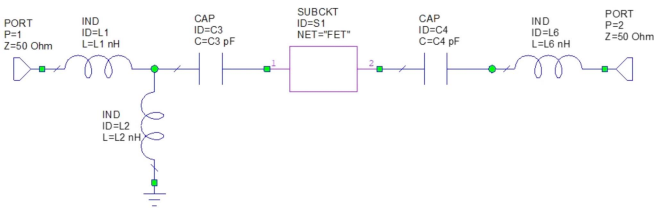

FIGURE 15. Matching circuit for the optimized 10% bandwidth LNA stage. The matching section parameters are $L_1 = 0.761$ nH, $L_2 = 2.231$ nH, $C_3 = 0.096$ pF, $C_4 = 0.365$ pF, $L_6 = 0.149$ nH.

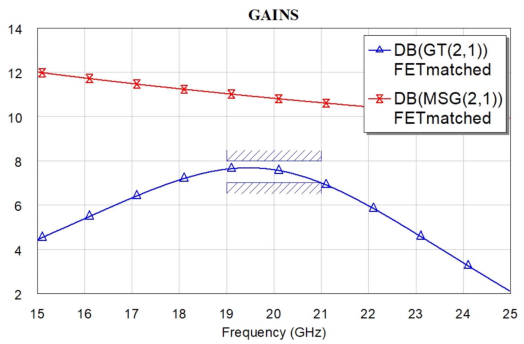

FIGURE 16. Transducer gain and maximum stable gain for the 10% bandwidth matched LNA stage shown in Fig. 15. The horizontal segment with upper diagonal strips denotes the optimization mask.

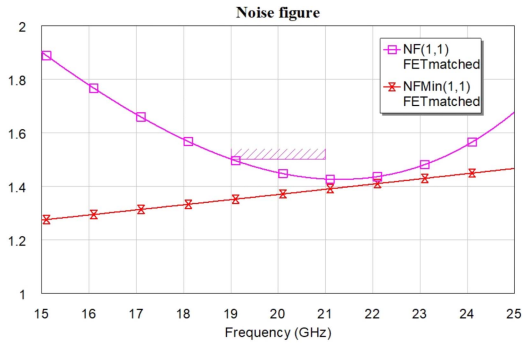

FIGURE 17. Noise figure and minimum noise figure for the 10% bandwidth matched LNA stage shown in Fig. 15. The horizontal segment with upper diagonal strips denotes the optimization mask.

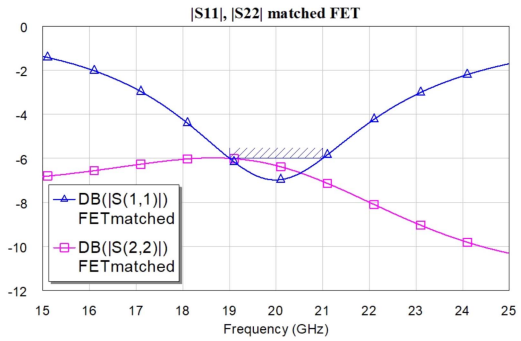

FIGURE 18. Input and output reflection coefficients for the 10% bandwidth matched LNA stage shown in Fig. 15. The horizontal segment with upper diagonal strips denotes the optimization mask.

the minimum input and output reflection coefficients are equal to −7.38 dB at 19 GHz. To implement the circuit we use the matching sections in Fig. 15, and impose, as the optimization goals on the whole design bandwidth (19–21 GHz), an input and output reflection coefficient (at ports 1 and 2 of the device cascaded with matching sections) below −6 dB, transducer gain between 6 and 7 dB, and, as already mentioned, NF < 1.5. The optimization of the matching circuit leads to the results reported in Figs. 16–18, showing that the design goals have been attained. Since $|S_{11}| < 1$ and $|S_{22}| < 1$ from 15 GHz to 25 GHz, in that interval the two-port operates in the stable region; out-of-band stabilization, not discussed here for brevity, could be of course needed outside this range, in particular at lower frequencies.

Notice that the preliminary knowledge of the theoretical bounds to matching is fundamental in setting reasonable and physically implementable optimization goals from the frequency-dependent stability factor K, immediately excluding optimization goals that are physically impossible (e.g., requiring $|S_{22}| = 0$, i.e., $\alpha = 0$, when $K \leq 0$).

C. LNA DESIGN STRATEGY

On the basis of the discussion presented in Sections VI-A and VI-B, we can outline the proposed strategy for design of an open-loop LNA stage exploiting conditionally stable devices as follows.

For **narrowband (single frequency) design**, given the device stability factor, we estimate the minimum input and ouput reflection coefficients for different values of the mismatch ratio α and select the α value yielding small enough reflection coefficients. If even for $\alpha = 1$ matching is unsatisfactory, we may increase K (and therefore improve the optimum matching value) through partial stabilization (e.g., exploiting an inductive feedback topology [5]), or use a balanced configuration [15] at the expense on some NF penalty. If a convenient α

value has been found, the matching sections can be optimized through CAD using as optimization goals the theoretical minima for $|S_{11}|$ and $|S_{22}|$ and the minimum NF. This leads to the selection of an optimum solution for matching that is also the closest one to the optimum noise source reflection coefficient, see the solutions corresponding to point C (Fig. 9) or D (Fig. 11) as discussed in Section VI-A. All solutions having optimum reflection coefficient are characterized by the same transducer gain.[6]

For **wideband design**, the theoretical minimum reflection coefficients are analyzed as a function of frequency for different values of α, selecting the mismatch ratio in order to obtain, at the frequency where the optimum matching is worst (typically, at the lowest frequency), an acceptable input and output mismatch. If this is not the case, the same steps as in narrowband design (e.g., partial stabilization) can be carried out. Then, optimization on the design bandwidth is performed imposing an input and output mismatch close to the theoretical values, a NF suitably larger that the minimum NF in the band, and a flat enough gain. Also in this case, the previous knowledge of the theoretical minima is essential, in particular for arbitrary values of α, to properly drive the optimization process by setting appropriate and realizable goals.

We finally remark that using a conditionally stable device may also help in obtaining a more wideband design, as expected from the Fano-Bode limit [16].

VII. CONCLUSION

The article derives a lower bound to the input and output mismatch of a conditionally stable two-port that only depends, in a simple way, on the stability factor K and on the mismatch ratio α assumed between the two ports, provided that condition $-\alpha \le K \le 1$ is met. As expected, the minimum mismatch increases with decreasing K, i.e., with increasing potential instability. The minimum mismatch condition is implemented by cascading the two-port with reactive matching sections, which can be designed by numerical optimization. It is also shown that the minimum mismatch condition is unique in terms of magnitude, but that an infinity of solutions can be obtained by varying the phase of the input and output reflection coefficients. The application of the theory to the design of low-noise amplifiers based on potentially in-band unstable devices is discussed through CAD examples.

APPENDIX A

In this section we show that both the constant operational gain and mismatch curves in Figs. 2 and 3, respectively, are circles, and that they coincide (i.e., Γ'_L corresponding to the same $|\Gamma'_{K,\text{out}}|$ also have the same G_p).

In fact, the transformation chain leading from the Γ'_L to the $\Gamma'_{K,\text{out}}$ plane ($\Gamma'_L \to \Gamma'_{\text{in}} \to Z'_{\text{in}} \to Z'^{*}_{\text{in}} \to Z'_{\text{out}} \to \Gamma'_{K,\text{out}}$) is a *bilinear* (or Möbius) transformation [17] where circles and straight lines are transformed into circles and straight lines; moreover, the two points where all constant $|\Gamma'_{K,\text{out}}|$ and G_p circles cross the unit circle of the Γ'_L plane (the *invariant points* discussed in [18, Sec. 10.7, p.751]) coincide. To prove this, notice that $|\Gamma'_{K,\text{out}}| = 1$ on two circles of the Γ'_L plane, the first being the unit circle, where Z'_L is reactive, and the second being the circle (crossing the unit circle and partly lying outside the Smith chart), where Z'_{out} is reactive, leading to unit magnitude $\Gamma'_{K,\text{out}}$ also when the reference impedance Z'_L is arbitrary. The two loci are indicated in Fig. 2 by a thicker red trace. The two conditions are simultaneously met in the invariant points, the first one implying that $P_L \to 0$ (since the load is reactive), the second one, together with the first one, that $P_{\text{in}} \to 0$ (since in the equivalent two-port circuit seen at the output port, no power is dissipated within the two port due to the reactive Z'_{out}, nor is transferred to the load, that is reactive, implying that $P_{\text{in}} \to 0$; this is confirmed by the fact that in the invariant points also $|\Gamma'_{\text{in}}| = 1$). However, conditions $P_{\text{in}} \to 0$ and $P_{\text{out}} \to 0$ are the same that characterize the invariant points of G_p, see [18, Sec. 10.7, p.751]. Thus, since two families of circles passing through the same two points must coincide, the level curves of G_p and $|\Gamma'_{K,\text{out}}|$ are the same.

APPENDIX B

Let us denote the two solutions of (9) as Γ^2_- and Γ^2_+, $\Gamma^2_+ \ge \Gamma^2_-$:

$$\Gamma^2_{-,+} = a \mp b$$

where the parameters a and b are defined in (11) and (12), respectively. By inspection, the argument of the square root in the definition of b, see (12), is certainly positive for $K \ge -\alpha \ge -(\alpha + \alpha^{-1})/2$ and $0 \le \alpha \le 1$; thus Γ^2_- and Γ^2_+ are both real. From (9), the product $\Gamma^2_-\Gamma^2_+$ is:

$$\Gamma^2_-\Gamma^2_+ = a^2 - b^2 = \frac{1 + |A|^2 - 2\,|A|\,K}{\alpha^2} \ge 0, \quad K \le 1$$

since, as shown in the discussion following (4), $1 + |A|^2 - 2|A|K \ge 0$ for $|A| \ge 0$, $K \le 1$; thus, for $-\alpha \le K \le 1$, Γ^2_- and Γ^2_+ certainly are real and have the same sign.[7] Since $\Gamma^2_+ \ge 0$ as the sum of two positive terms, also $\Gamma^2_- \ge 0$. Thus, the minimization Γ_a can be performed on its square. Consider now that, from (9), $\Gamma^2_- + \Gamma^2_+$ is given by:

$$\Gamma^2_- + \Gamma^2_+ = 2a = \frac{1 + \alpha^2 + 2\alpha\,|A|}{\alpha^2} = \\ = 1 + \frac{1}{\alpha^2} + \frac{2\,|A|}{\alpha} \ge 2, \quad 0 \le \alpha \le 1, |A| \ge 0$$

Thus, since $\Gamma^2_+ \ge \Gamma^2_-$, $\Gamma^2_+ \ge 1$ necessarily, and therefore the only solution that may be within the Smith chart is Γ^2_-, while the solution Γ^2_+ has to be discarded.

[6]The proposed strategy is quite different from that followed in LNA single-frequency design with unconditionally stable devices, where, in the gain/NF tradeoff, the optimum input mismatch is zero, corresponding to the maximum gain; this implies that input matching and gain optimization occur together. Here, the (nonzero) optimum input mismatch is known, but the gain may increase or decrease with decreasing NF depending on the position of Γ_{NGopt} with respect to the locus of minimum input mismatch.

[7]The limitation $-\alpha \le K \le 1$ is consistent with the discussion in Appendix C.

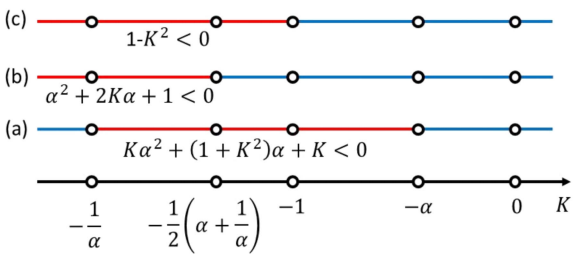

FIGURE 19. Graphical representation of the intervals defined in the discussion of Appendix C. (a) refers to the numerator of $|A|_{opt}$; (b), to the denominator of $|A|_{opt}$ and Γ^2_{min}; (c), to the numerator of Γ^2_{min}.

APPENDIX C

We discuss here the limitation $-\alpha \leq K$, starting from (13) that is repeated here for easier reference:

$$|A|_{\text{opt}} = \frac{K\alpha^2 + \left(1+K^2\right)\alpha + K}{\alpha^2 + 2K\alpha + 1}$$

Let us discuss the behavior of $|A|_{\text{opt}}$ as a function of K, with the help of the graphical representation in Fig. 19. Taking into account that the numerator is negative in the interval:

$$-\frac{1}{\alpha} < K < -\alpha$$

that the denominator is negative in the interval:

$$K < -\frac{1}{2}\left(\alpha + \frac{1}{\alpha}\right)$$

and that, see again Fig. 19:

$$-\frac{1}{\alpha} \leq -\frac{1}{2}\left(\alpha + \frac{1}{\alpha}\right) \leq -1 \leq -\alpha \leq 0$$

we obtain that certainly $|A|_{\text{opt}} \leq 0$ in the interval $-1 \leq K \leq -\alpha$ where the numerator is negative and the denominator is positive. Therefore, we have the limitation $-\alpha \leq K$. Concerning the region $K < -1$ (that could be excluded *a-priori* with reference to [11], [12]), consider the optimum reflection coefficient squared from (14), reported here for easier reference:

$$\Gamma^2_{\text{min}} = \frac{1-K^2}{\alpha^2 + 2K\alpha + 1}$$

For $K \leq -1$ the numerator is always negative while the denominator is positive for:

$$-\frac{1}{2}\left(\alpha + \frac{1}{\alpha}\right) < K < -1$$

In this region, therefore, $\Gamma^2_{\text{min}} \leq 0$ and the solution is not acceptable. For:

$$K < -\frac{1}{2}\left(\alpha + \frac{1}{\alpha}\right) \tag{20}$$

both the numerator and the denominator are negative, so that $\Gamma^2_{\text{min}} > 0$. However, we can show that in this region $\Gamma^2_{\text{min}} > 1$, i.e., the optimum reflection coefficient lies outside the unit circle of the Smith chart. In fact, if the inequality (20) holds, we have the following implication chain:

$$\frac{1-K^2}{\alpha^2 + 2K\alpha + 1} > 1 \rightarrow 1 - K^2 < \alpha^2 + 2K\alpha + 1 \rightarrow$$
$$\rightarrow \alpha^2 + 2K\alpha + K^2 = (\alpha + K)^2 > 0$$

In conclusion, no physical solution for Γ_{min} can exist for $K < -1$.

ACKNOWLEDGMENT

Helpful discussions with dr. Chiara Ramella and dr. Alberto Tibaldi of Politecnico di Torino, Department of Electronics and Telecommunications, are gratefully acknowledged.

REFERENCES

[1] M. Karp, "Power gain and stability," *IRE Trans. Circuit Theory*, vol. 4, no. 4, pp. 339–340, 1957.
[2] J. Rollett, "Stability and power-gain invariants of linear twoports," *IRE Trans. Circuit Theory*, vol. 9, no. 1, pp. 29–32, 1962.
[3] G. Gonzales, *Microwave Transistor Amplifiers: Analysis and Design*, 2nd ed. Englewood Cliffs, NJ, USA: Prentice-Hall, 1996.
[4] L. Nevin and R. Wong, "L-band GaAs FET amplifier," in *Proc. 8th Eur. Microw. Conf.*, 1978, pp. 140–145.
[5] D. D. Henkes, "LNA design uses series feedback to achieve simultaneous low input VSWR and low noise," *Appl. Microw. Wireless*, vol. 10, pp. 26–33, 1998.
[6] "Microwave encyclopedia - unstable amplifier examples," 2023. [Online]. Available: https://www.microwaves101.com/encyclopedias/unstable-amplifier-examples
[7] P. Owens and D. Woods, "Reappraisal of the unconditional stability criteria for active 2-port networks in terms of S parameters," *Electron. Lett.*, vol. 10, no. 6, 1970, Art. no. 315.
[8] D. Woods, "Reappraisal of the unconditional stability criteria for active 2-port networks in terms of S parameters," *IEEE Trans. Circuits Syst.*, vol. 23, no. 2, pp. 73–81, Feb. 1976.
[9] M. L. Edwards and J. H. Sinsky, "A new criterion for linear 2-port stability using a single geometrically derived parameter," *IEEE Trans. Microw. Theory Techn.*, vol. 40, no. 12, pp. 2303–2311, Dec. 1992.
[10] K. Kurokawa, "Power waves and the scattering matrix," *IEEE Trans. Microw. Theory Techn.*, vol. 13, no. 2, pp. 194–202, Mar. 1965.
[11] G. Lombardi and B. Neri, "On the relationships between input and output stability in two-ports," *IEEE Trans. Circuits Syst. I, Reg. Papers*, vol. 66, no. 7, pp. 2489–2495, Jul. 2019.
[12] G. Lombardi and B. Neri, "Microwave circuit conditional stability: Two-parameter criteria," *IEEE Trans. Circuits Syst. II, Exp. Briefs*, vol. 67, no. 12, pp. 2913–2917, Dec. 2020.
[13] J. M. Rollett, *Some Invariant Properties of linear Electrical Circuits*. Guildford, U.K.: Univ. Surrey, 1971.
[14] M. W. Pospieszalski, "Modeling of noise parameters of MESFETs and MODFETs and their frequency and temperature dependence," *IEEE Trans. Microw. Theory Techn.*, vol. 37, no. 9, pp. 1340–1350, Sep. 1989.
[15] A. A. Coskun and A. Atalar, "Noise figure of a balanced amplifier," *IEEE Trans. Circuits Syst. II, Exp. Briefs*, vol. 65, no. 9, pp. 1129–1133, Sep. 2018.
[16] R. Fano, "Theoretical limitations on the broadband matching of arbitrary impedances," *J. Franklin Inst.*, vol. 249, no. 1, pp. 57–83, 1950.
[17] Wikipedia contributors, "Möbius transformation–Wikipedia, the free encyclopedia," 2023. Accessed: May, 3, 2023. [Online]. Available: https://en.wikipedia.org/w/index.php?title=M%C3%B6bius_transformation&oldid=1151068281
[18] R. E. Collin, *Foundations for Microwave Engineering*, 2nd ed. Hoboken, NJ, USA: Wiley, 2001.